Structural and Functional Characterization of *Mycobacterium tuberculosis* CmtR, a Pb^{II}/Cd^{II}-Sensing SmtB/ArsR Metalloregulatory Repressor†

Yun Wang,‡ Lars Hemmingsen,§ and David P. Giedroc*,‡

Department of Biochemistry and Biophysics, 2128 TAMU, Texas A&M University, College Station, Texas 77843-2128, and Department of Natural Science, The Royal Veterinary and Agricultural University, Thorvaldsensvej 40, DK-1871 Frederiksberg C, Denmark

Received January 15, 2005; Revised Manuscript Received May 6, 2005

ABSTRACT: The SmtB/ArsR family of prokaryotic metalloregulators are winged-helix transcriptional repressors that collectively provide resistance to a wide range of both biologically required and toxic heavy-metal ions. CmtR is a recently described Cd^{II}/Pb^{II} regulator expressed in *Mycobacterium tuberculosis* that is structurally distinct from the well-characterized SmtB/ArsR Cd^{II}/Pb^{II} sensor, *Staphylococcus aureus* plasmid pI258-encoded CadC. From functional analyses and a multiple sequence alignment of CmtR paralogs, *M. tuberculosis* CmtR is proposed to bind Pb^{II} and Cd^{II} via coordination by Cys57, Cys61, and Cys102 [Cavet et al. (2003) *J. Biol. Chem.* **278**, 44560−44566]. We establish here that both wild-type and C102S CmtR are homodimers and bind Cd^{II} and Pb^{II} via formation of cysteine thiolate-rich coordination bonds. UV−vis optical spectroscopy, ^{113}Cd NMR spectroscopy ($\delta = 480$ ppm), and ^{111m}Cd perturbed angular correlation (PAC) spectroscopy suggest two or three thiolate donors in the wild-type protein. Cys57 and Cys61 anchor the coordination complex, while Cys102 plays only an accessory role in stabilizing the metal chelate in the free protein because C102S CmtR binds Cd^{II} and Zn^{II} with only ≈10−20-fold lower affinity relative to wild-type CmtR but ≈100−1000-fold lower for Pb^{II}. Quantitative investigation of CmtR-*cmt* O/P binding equilibria using fluorescence anisotropy, however, reveals that Cys102 functions as a key allosteric metal ligand, because substitution of Cys102 abrogates disassembly of oligomeric CmtR-*cmt* O/P oligomeric complexes. The implications of these findings on the evolution of distinct metal-sensing sites in a family of homologous proteins are discussed.

The first-row transition-metal ions, including zinc, copper, iron, nickel, manganese, and cobalt, play a wide range of biological roles essential for cell survival. Although these are often found at relatively low concentrations, they can be selectively accumulated by cells. Some transition-metal ions, e.g., Cu and Fe, function naturally as enzyme cofactors but, when present in excess, can catalyze cytotoxic reactions via redox chemistry (*3*). To maintain an intracellular pool of these essential metal ions compatible with cellular needs, all cells, from bacteria to plants to eukaryotic cells, have evolved homoeostasis mechanisms that balance the expression of genes that encode proteins involved in specific metal uptake and export storage of essential metal ions (*4*, *5*). The same regulatory mechanisms are exploited in many cases to provide resistance to heavy-metal pollutants, including cadmium, lead, mercury, and arsenic (*6*−*8*).

Members of the SmtB/ArsR family of prokaryotic metalloregulatory transcriptional repressors regulate intracellular metal-ion concentrations under conditions of metal excess by functioning as metalloregulatory sensors (for a recent review, see ref *7*). These repressors sense di- and multivalent heavy-metal ions and regulate the expression of operons that typically encode metal-specific efflux pumps, membrane-bound transporters, or intracellular chelators, e.g., metallothioneins (*7*, *9*). SmtB/ArsR family members appear to act exclusively as transcriptional repressors of metal-resistance proteins (*7*). This contrasts to another class of prokaryotic metal sensors, the paradigm for which is the Hg^{II} sensor MerR (*10*) that becomes a potent transcriptional activator in the presence of bound metals (*8*). Transcription is repressed when the apo-SmtB/ArsR proteins are specifically bound to the operator/promoter (O/P)[1] region (*7*) and is derepressed upon specific metal binding. Derepression is mediated by typically strong allosteric negative regulation of O/P binding.

SmtB/ArsR metal sensors are widely distributed throughout pathogenic and nonpathogenic bacteria, including Gram negative and Gram positive eubacteria, archebacteria, cyanobacteria, and actinomycetes, e.g., mycobacteria, corynebacteria, and *Streptomyces* strains. Metal-sensor-dependent regulation of the transcription of these operons confers resistance to a wide range of heavy-metal ions including Zn^{II} (*11*), Co^{II}, Ni^{II} (*12*), and Cu^{I}/Ag^{I} (*13*), as well as Cd^{II}, Pb^{II} (*14*), Bi^{III} (*15*), As^{III}, and Sb^{III} (*7*, *16*).

The best characterized Cd^{II}/Pb^{II} sensor is *Staphylococcus aureus* plasmid pI258-encoded CadC, which regulates the expression of a P_{1B}-type ATPase metal efflux pump, CadA.

† This work was supported by grants from the National Institutes of Health (GM042569) and the Robert A. Welch Foundation (A-1295).

* To whom correspondence should be addressed. E-mail: giedroc@tamu.edu. Telephone: 979-845-4231. Fax: 979-845-4946.

‡ Texas A&M University.

§ The Royal Veterinary and Agricultural University.

[1] Abbreviations: DTNB, 5,5′-dithiobis(2-nitrobenzoic acid); LMCT, ligand−metal charge transfer; O/P, operator/promoter.

10.1021/bi050094v CCC: $30.25 © 2005 American Chemical Society
Published on Web 06/04/2005

In CadCs and other closely related thiophilic metal sensors, metals bind to an α3N site that adopts a trigonal or distorted tetrahedral geometry, formed by three invariant Cys ligands, one from the N-terminal unstructured region (a fourth conserved Cys is often found here as well) and two derived from a ...CVC... sequence in the putative α3 helix (*14*, *15*, *17*−*19*). pI258 CadC binds Cd^{II} and Pb^{II} to the α3N site that is necessary and sufficient for metalloregulation of the *cad* O/P binding (*18*). In contrast, the C-terminal α5 helix donates a mixture of carboxylate and imidazole ligands to a pair of symmetry-related α5 sites that form tetrahedral complexes in the Zn^{II} sensors SmtB and CzrA and octahedral coordination complexes in Ni^{II} sensor *Mycobacterium tuberculosis* NmtR (*11*, *20*, *21*). In SmtB and CzrA, Zn^{II} binding drives a quaternary structural switch that is mediated by direct hydrogen bonding of a nonliganding face of a coordinating histidine (Nϵ2 of His117 in SmtB) to a backbone carbonyl oxygen (Arg87′) found in the turn region between the α4 helix and the β hairpin of the opposite subunit. Another distinctive characteristic of SmtB/ArsR sensors is the α4 helix, which is highly conserved in all SmtB/ArsR sensors as part of the putative protein α3−turn−αR helix−turn−helix DNA-binding motif (*2*, *22*).

M. tuberculosis H37Rv CmtR (Rv1994c ORF) is a recently described Pb^{II}/Cd^{II}-specific SmtB/ArsR sensor (*1*) that lacks both typical α3N and α5 sites and therefore possesses novel metal-sensing sites structurally distinct from *S. aureus* pI258 CadC (*17*). Previous *in vivo* β-galactosidase assays carried out by *Mycobacterium smegmatis* revealed that CmtR is capable of metalloregulating reporter gene expression in response to Cd^{II} and Pb^{II} salts, but not Zn^{II}, a property that distinguishes CmtR from other Cd^{II}/Pb^{II} metal sensors. Other metal ions, notably nickel, cobalt, iron, copper, and mercury, failed to induce *cmtR-lacZ* gene expression at their maximum permissive concentrations in mycobacteria (*1*). CmtA, the protein whose expression is thought to be regulated by CmtR, is closely related to *S. aureus* CadA and *Escherichia coli* ZntA, both of which are well-characterized $Zn^{II}/Cd^{II}/Pb^{II}$ P_{1B}-type ATPase efflux pumps (*23*, *24*). Reporter gene assays were also performed with several CmtR variants (*1*). Among the six cysteine residues in CmtR, only Cys57, Cys61, and Cys102 were shown to be essential for Cd^{II}-mediated transcriptional derepression in *M. smegmatis* (*1*), shown mapped onto a homology model of CmtR (Figure 1A); this finding is consistent with the fact only these three Cys are absolutely conserved in putative CmtR homologues from other bacteria (Figure 1B). Note that the CmtR homology model (Figure 1A) reveals that Cys61 is just N-terminal to Arg87 of SmtB, a key allosteric residue in SmtB (*2*). Six of the nine putative CmtR homologues are found in the genomes of actinomycetes and include a previously characterized Hg^{II} sensor from *Streptomyces lividans* termed MerR (*25*). A putative O/P region that forms a binding site for CmtR was also proposed by a gel-mobility shift assay in that study (*1*).

To gain insight into the mechanism of metalloregulation by CmtR, we have quantitatively characterized the metal- and DNA-binding properties of nearly fully reduced wild-type CmtR and a C102S substitution mutant. Of particular interest was the extent to which CmtR binds Zn^{II}, because this metal fails to induce transcription *in vivo* (*1*). In this paper, we establish that both wild-type and C102S CmtRs are homodimeric and bind Cd^{II}, Pb^{II}, and Zn^{II} tightly via

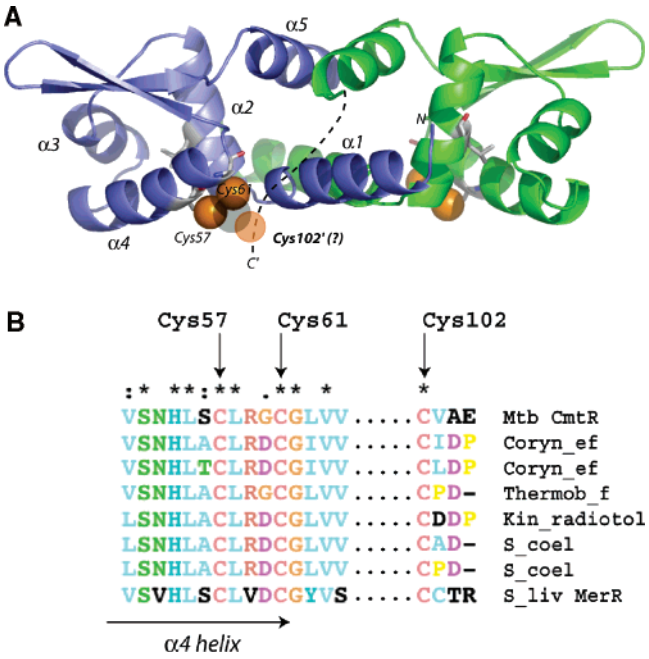

FIGURE 1: (A) Homology model of the CmtR homodimer based on the crystal structure of the apo-SmtB structure (*2*, *22*). One CmtR protomer is shaded blue and the other green. The carboxyl terminus of CmtR cannot be modeled and is represented by a dotted line. Important cysteine residues are labeled. (B) Two windows derived from multiple sequence alignment of *M. tuberculosis* CmtR and putative homologues. Each homologue has three conserved cysteines that correspond to Cys57, Cys61, and Cys102 in the *M. tuberculosis* CmtR sequence.

formation of cysteine thiolate coordination bonds with an apparent metal-binding stoichiometry of 0.5−1.0 per protomer, in contrast to previous findings (*1*). C102S CmtR binds Cd^{II} and Zn^{II} with only a slightly lower affinity relative to wild-type CmtR (≈10−20-fold) and ∼100−1000-fold lower in Pb^{II} binding. UV−vis optical spectroscopy, ^{113}Cd NMR spectroscopy, and ^{111m}Cd PAC spectroscopy (*26*) suggest that the coordination complex is anchored by two strong thiolate donor atoms, proposed to be Cys57 and Cys61, while Cys102 makes a smaller but measurable contribution to the ligand−metal charge transfer (LMCT) intensity in the ultraviolet. The *cmt* O/P binding affinities of apo-wild-type and apo-C102S CmtRs are similar, but Cd^{II} strongly negatively regulates the assembly of higher order (2:1 and 3:1) wild-type CmtR homodimer/*cmt* O/P complexes but not those formed by C102S CmtR. These experiments reveal that Cys102, while making a minor contribution to metal-binding affinity, is critically required for allosteric regulation of *cmt* O/P binding. These findings are discussed in the context of previous work on the paradigm Cd^{II}/Pb^{II} sensor *S. aureus* pI258 CadC.

MATERIALS AND METHODS

Chemicals. All buffers were prepared using Milli-Q doubly distilled deionized water. MES, Tris, HEPES, and bis-Tris buffer salts, ammonium sulfate, and 5,5′-dithiobis(2-nitrobenzoic acid) (DTNB) were purchased from Sigma. Chromatography materials were obtained from Pharmacia Biotech. Ultrapure cadmium(II) chloride and lead(II) chloride were acquired from Johnson Matthey. HEPES-d_{18} and D_2O were obtained from Cambridge Isotopes.

Construction of Wild-Type and C102S CmtR Overexpression Plasmids. To create pET3a-CmtR, the CmtR-coding region was amplified by PCR from *M. tuberculosis* H37Rv genomic DNA using primers I (5′-GAGTCCATATGCTGACGTGTGAG-3′) and II (5′-GTCATGGATCCTCATCAGCTACCTGTC-3′) and cloned into pET3a (Novagen) between the *Bam*HI and *Nde*I restriction sites using standard cloning techniques. The C102S CmtR mutant was generated by site-directed mutagenesis method using the QuikChange kit (Stratagene) and primers III (5′-GATACCGACCAACCCTCTGTC-3′) and IV (5′-GACAGAGGGTTGGTCGGTATC-3′) and pET3a-CmtR as a template.

Purification of Wild-Type and Mutant CmtRs. pET3a-CmtR-transformed *E. coli* BL21(DE3)/pLysS was grown on a 1.5% LB agar plate containing 0.1 mg/mL ampicillin at 37 °C. A single colony was used for 200 mL of overnight seed culture (37 °C), which was subsequently used to inoculate 9 L of LB containing 0.1 mg/mL ampicillin. The cells were grown at 37 °C with vigorous aeration to an OD of 0.5−0.6 at 600 nm, after which time 0.4 mM IPTG was added to induce the expression of CmtR. Cells were harvested by low-speed centrifugation, and the wet cell paste was used for purification. The purification of CmtR was largely adapted from prior procedures for pI258 CadC (*14*), except that 5 mM DTT was used throughout and the final dialysis carried out in the anaerobic chamber was against 10 mM HEPES and 0.40 M NaCl at pH 7.0. After purification, overloaded SDS−PAGE gels showed a single band at the anticipated molecular weight (12.5 kDa). The concentration of CmtR was determined using the calculated molar extinction coefficient at 280 nm of 5220 M^{-1} cm^{-1} (*27*). Purified CmtR was stored at −80 °C in an anaerobic environment in small aliquots in sealed tubes. C102S CmtR was purified using the same method except that *E. coli* Rosetta (DE3) cells were used for protein expression.

Free Thiol Determination. A standard DTNB colorimetric assay was used to determine the number of free thiols in CmtR (*28*). A total of 25 μL of 2.5 mM DTNB solution was added separately into 400 μL of 10−15 μM CmtR. After incubation for 30 min in the anaerobic chamber, the concentration of thiolate anion was quantified at 412 nm (ϵ = 13 600 M^{-1} cm^{-1}) after subtraction of the absorbance of the final dialysis buffer with the same concentration of DTNB. The calculated number of free thiols in wild-type and C102S CmtR was found to be 5.5 ± 0.2 (6 expected) and 4.3 ± 0.2 (5 expected) free thiols per monomer.

Atomic Absorption Spectroscopy. The concentrations of all metal titrants were determined using a Perkin−Elmer AAnalyst 700 atomic absorption spectrophotometer operating in flame mode using different hollow cathode lamps specific for each metal (*28*). Zn^{II} was detected at 213.9 nm (slit = 0.7 nm); Cd^{II} was detected at 228.8 nm (slit = 0.7 nm); and Pb^{II} was detected at 283.3 nm (slit = 0.7 nm).

Analytical Sedimentation Equilibrium Ultracentrifugation. A Beckman Optima XL-A analytical ultracentrifuge was used to run all experiments (*14*), with the rotor speed set to 20 000 rpm at 25.0 °C. Ultracentrifuge cells were assembled in the anaerobic glovebox and contained 12 μM apo-wild-type CmtR or C102S CmtR. Sedimentation equilibrium data were acquired and evaluated by a nonlinear least-squares fitting program, Microcal Origin. The partial specific volume (ν) of 0.736 mL/g for CmtR, 0.7361 mL/g for C102S CmtR, and a buffer density (ρ) of 1.0 g/mL was used in the analysis via global simultaneous fitting to a single ideal species model by Ultrascan. The lower limit of the dimerization equilibrium constant, K_{dimer}, was calculated assuming $2\,P \leftrightarrow P_2$ and that $[(1-P)/(1-0.5P)]M_r^{P} + [0.5P/(1-0.5P)]M_r^{P_2} = M_r^{observed}$, where P is the fractional population of monomer that self-associates into the dimer and K_{dimer} (lower limit) = $(0.5\,PC)/[(1-P)C]^2$, where C is the total protein concentration.

Cd^{II} and Pb^{II} Optical Absorption Spectroscopy. All metal-binding experiments were carried out anaerobically at ambient temperature (~25 °C) using a Hewlett−Packard model 8452A spectrophotometer (*14*). For Cd^{II} titrations, apoproteins were diluted using a final dialysis buffer S to ≈50 μM in 800 μL and loaded into an anaerobic cuvette fitted with a Hamilton gastight adjustable volume syringe containing 0.5 mM Cd^{II} titrant in the glovebox. Complete optical spectra of apoprotein were collected from 200 to 900 nm for 1−2 min after each addition of a known aliquot (5−15 μL) of Cd^{II}. Corrected spectra were obtained by subtraction of the apoprotein spectra from each spectrum obtained after addition of the metal ion and further corrected for dilution. The binding isotherms were fit to a 1:1 binding model (Dynafit) to obtain a lower limit for K_{Cd}. Pb^{II} titrations were done in exactly the same way except that 10 mM bis-Tris and 0.4 M NaCl at pH 7.0 were used as the buffer. Bis-Tris is a weak chelating buffer that can prevent excess Pb^{II} from forming $Pb^{II}(OH)_2$ precipitate (*29*). Metal competition experiments performed with either EDTA or EGTA were carried out as described above except that the 100−300 μM chelator was present. The conditional stability constants for various metal−chelator complexes were calculated under these conditions essentially as described (*30*, *31*) with $K_{Cd}^{EDTA} = 3.2 \times 10^{12}$ M^{-1} and $K_{Pb}^{EGTA} = 1.38 \times 10^{10}$ M^{-1}. The resulting optical data were fitted to a simple competition model using DynaFit.

Zn^{II}-Binding Experiments. The zinc chelator dye magfura-2 ($K_{Zn} = 5.0 \times 10^7$ M^{-1} at pH 7.0 and 25 °C) (*21*) was used as a colorimetric competitor for Zn^{II} binding by wild-type and C102S CmtR as previously described (*21*). For wild-type CmtR, 20 μM CmtR and 18.8 μM magfura-2 were used; for C102S CmtR, 19.8 μM protein and 19 μM magfura-2 were used. The data were fit to a competitive binding model using DynaFit to determine the zinc-binding affinity K_{Zn} for both proteins.

^{113}Cd NMR Spectroscopy. The ^{113}Cd NMR spectrum of wild-type CmtR was recorded as previously described (*14*). The final concentration of $^{113}Cd^{II}$-bound CmtR was determined by optical spectroscopy to be 0.8 mM.

Perturbed Angular Correlation (PAC) Spectroscopy. PAC spectroscopy was carried out at 1 ± 2 °C, controlled by a Peltier element. The radioactive ^{111m}Cd isotope was produced on the day of the experiment at University Hospital cyclotron (Copenhagen), typically 500 MBq at the end of production, and extracted as described previously (*32*). In addition, an HPLC separation (using a TESSEK HEMA 40Q PEEK 7.5 × 75 mm anion-exchange column) of the cadmium from other metal ions, most notably zinc ions, was carried out. The ^{111m}Cd-containing fractions were pooled, evaporated to about 50 μL, and mixed with nonradioactive cadmium acetate and MES buffer. The protein was added; the sample was left to equilibrate for 10 min to allow for metal binding; and 55% (w/w) sucrose was added to slow rotational tumbling

of the molecules. The samples were purged with argon and either used immediately after preparation or left on ice for up to 3 h until the measurement was initiated. All buffers were purged with argon and treated so as to lower metal contamination. The final volume of the samples ranged between 0.05 and 0.2 mL with concentrations of 51 μM protein, 10 μM Cd^{II}, 53 mM MES, 430 mM NaCl, and 55% (w/w) sucrose and pH as indicated in Table 1. The pH was measured at room temperature the day after the PAC experiment.

The theoretical and technical aspects of PAC spectroscopy are reviewed in detail in ref *33* with particular emphasis on biological applications in ref *26*. The radioactive ^{111m}Cd isotope is used, exploiting the angular correlation between the two γ-rays emitted in the nuclear decay. This angular correlation is perturbed by the nuclear quadrupole interaction between the nuclear electric quadrupole moment and the electric field gradient from the surrounding charge distribution. Measuring this perturbed angular correlation provides a fingerprint of the metal-ion-binding site structure (*26*, *33*). The experimental perturbation function, $A_2G_2(t)$, was constructed from coincidence spectra for all 30 combinations of six detectors mounted so that they face the six sides of a cube (*32*). The background due to accidental coincidences was subtracted in each spectrum, and time calibration was carried out using a ^{75}Se source. The theoretical expression for the perturbation function for randomly oriented molecules contains five parameters, which were fitted to the experimental perturbation function using a conventional χ^2 method (*32*). The parameters fitted to the experimental data are ω_0, a measure of the nuclear quadrupole interaction strength; η, the so-called asymmetry parameter (always between 0 and 1 in magnitude and 0 for axially symmetric complexes); $\Delta\omega_0/\omega_0$, the frequency spread, assuming a Gaussian distribution around ω_0 with a width of $\Delta\omega_0/\omega_0$, describing small structural variations among molecules; τ_c, the rotational correlation time of the molecule; and *A*, the amplitude of the signal. The fits were carried out using 400 data points, except the first 5 points because of systematic errors. For the C102S CmtR mutant, the rotational correlation time was constrained to be the same for the two NQIs recovered from the fits.

Fluorescence Anisotropy. All fluorescence anisotropy experiments were carried out with an ISS PC1 photon-counting spectrofluorometer operating in the L format. A 40-mer, double-stranded *cmt* O/P oligonucleotide (*1*) (Qiagen) used was 5′-end-labeled with fluorescein as indicated on the sequence below:

5′-[F]-CAAA<u>TAGTACACCA</u>TATAC<u>TGGTATAACA</u>-GCAAGAGCTGA-3′

3′-GTTT<u>ATCATGTGGT</u>ATATG<u>ACCATATTGT</u>CGT-TCTCGACT-5′

The 10−5−10 inverted repeat previously proposed to be critical for the binding of CmtR is underlined (*1*). Apo-CmtRs or Cd^{II}−CmtRs (preformed stoichiometric complexes) were used as titrants into 1.8 mL of 20 or 80 nM *cmt* O/P at 25.0 °C. For the apoprotein titrations, the binding buffer contained 10 mM HEPES, 0.4 M NaCl, 1.0 mM DTT, and 50 μM EDTA at pH 7.0. For the Cd^{II}−protein titrations, EDTA was absent from the buffer and replaced by 10 μM Cd^{II}. Anisotropy data were fit using DynaFit to a dissociable dimer (P_2) model with a limiting 3:1 P_2D binding stoichiometry linked to the monomer−dimer equilibrium (*12*):

$$P + P \leftrightarrow P_2;\ K_{dimer}$$

$$P_2 + D \leftrightarrow P_2D;\ K_1$$

$$P_2 + P_2D \leftrightarrow (P_2)_2D;\ K_2$$

$$P_2 + (P_2)_2D \leftrightarrow (P_2)_3D;\ K_3$$

In these fits, K_{dimer} was fixed to the lower limits determined by analytical sedimentation equilibrium ultracentrifugation where $K_{dimer} = 1.7 \times 10^7\ M^{-1}$ for both wild-type CmtR and C102S CmtR. The characteristic anisotropy, r_i, for each $(P_2)_nD$ complex was estimated by stoichiometric additions of wild-type CmtR and C102S CmtR to a high concentration of *cmt* O/P fragment (10 μM). The results of these titrations gave $r_{P_2D} = 0.092$, $r_{(P_2)_2D} = 0.110$, and $r_{(P_2)_3D} = 0.135$ for wild-type CmtR and $r_{P_2D} = 0.104$, $r_{(P_2)_2D} = 0.120$, and $r_{(P_2)_3D} = 0.148$ for C102S CmtR, with the $r_D = 0.082$ for free DNA. Each r_i was treated as fixed parameters to obtain K_i for each binding step. If r_D was not exactly equal to 0.082 in any particular experiment, all r_i values were adjusted up or down accordingly, but by no more than 0.005 anisotropy units (*34*).

RESULTS

Assembly State of Wild-Type and C102S CmtR. Both CmtR variants were subjected to analytical equilibrium sedimentation ultracentrifugation at 20 000 rpm at 12 μM monomer concentration under conditions of pH and temperature (pH 7.0 and 25.0 °C) identical to the metal- and DNA-binding experiments. Absorbance was recorded at 237 nm, with the results shown in Figure 2. Each set of experimental data that had reached equilibrium was then subjected to a global simultaneous fit to a single ideal species model shown by a solid line. The apparent molecular weights obtained 24 750 (expected 25 956.1 g/mol) and 26 540 g/mol (expected 25 923.9 g/mol) for wild-type and C102S CmtR, respectively. These data reveal that both apo-CmtR and apo-C102S CmtR are stable homodimers under these conditions. Because the monomer concentration is too low under these conditions to accurately measure, only a lower limit of K_{dimer} of $1.7 \times 10^7\ M^{-1}$ could be obtained from these data.

Cd^{II} Optical Spectroscopy. Shown in Figure 3 are representative absorption spectra that result from anaerobic Cd^{II}-binding titration of ≈50 μM apo-wild-type CmtR (Figure 3A) and C102S CmtR (Figure 3B). Binding isotherms (insets) were obtained by plotting the corrected absorbance at 240 nm as a function of the [Cd^{II}]/[CmtR] or [Cd^{II}]/[C102S CmtR] ratio. As can be seen, both spectral titrations with Cd^{II} result in intense absorption in the ultraviolet, assignable to S^- to Cd^{II} LMCT transition. Cd^{II} binds with an apparent stoichiometry of ≈0.75 Cd^{II}/CmtR monomer in both cases. The simplest interpretation of a nonintegral stoichiometry is partial inactivation of metal sites because of some cysteine oxidation (see the Materials and Methods), as previously observed for CadC (*14*). We see no evidence for the presence of a second cysteine-containing Cd^{II} site in CmtR as

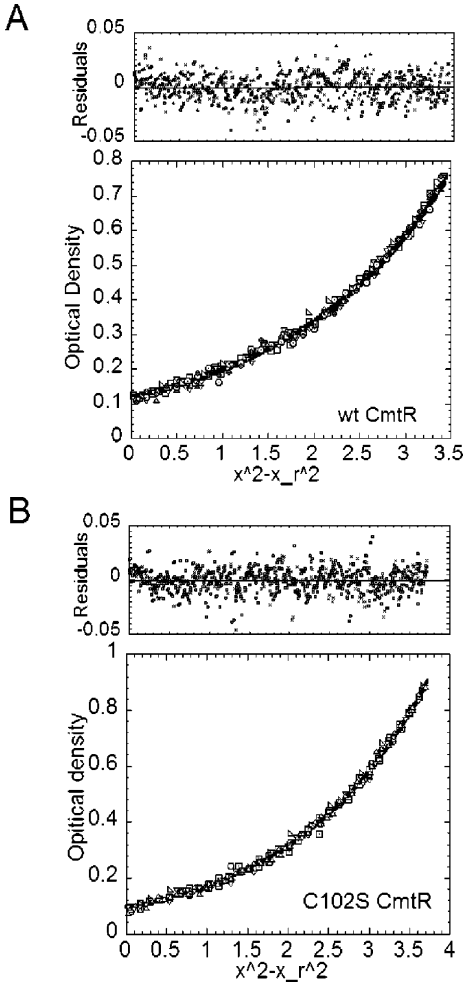

FIGURE 2: Analytical sedimentation equilibrium ultracentrifugation of (A) apo-wild-type CmtR and (B) apo-C102S CmtR. The protein concentration in each case was 12 μM monomer. Filled symbols represent an overlay of the data collected during the last five scans, indicative that equilibrium had been reached. The solid line represents the global simultaneous fit for a single ideal species model using Ultrascan. For wild-type CmtR, the fitted M_w is 24 750 D (theoretical dimer M_w = 25 956 D), variance = 1.5590 e^{-4}. For apo-C102S CmtR, the fitted M_w = 26 540 D (theoretical dimer M_w = 25 924 D), variance =1.1885 e^{-4}. Conditions: 10 mM HEPES, 0.4 M NaCl, and 0.1 mM EDTA at pH 7.0, 25 °C, and 20 000 rpm rotor speed.

found previously (*1*).[2] Molar absorptivities are ≈16 000 M^{-1} cm^{-1} for wild-type CmtR and ≈12 000 M^{-1} cm^{-1} for C102S CmtR, both of which are less intense than the tetrathiolate Cd^{II} coordination complex in pI258 CadC (*14*). The molar absorptivity is lower in the C102S mutant than in wild-type CmtR, consistent with a loss of cysteinate coordination; however, the change is somewhat smaller than expected in going from three to two coordinating cysteinates, assuming 5500 M^{-1} cm^{-1} for each Cd−S coordination bond (*35*−*37*).

[2] The reason for this discrepancy is unclear. The Cd^{II}-binding isotherm previously reported (*1*) seems indicative of very weak binding with K_{Cd} in the 10^5 M^{-1} range, in obvious contrast to the results reported here. This may be due to significant oxidation of CmtR cysteines during protein purification (no analytical data on this point was provided) and subsequent very weak metal binding. In multiple preparations of nearly fully reduced CmtR, we see no evidence for Cd^{II}-binding stoichiometries greater than 0.8 measured in an anaerobic atmosphere.

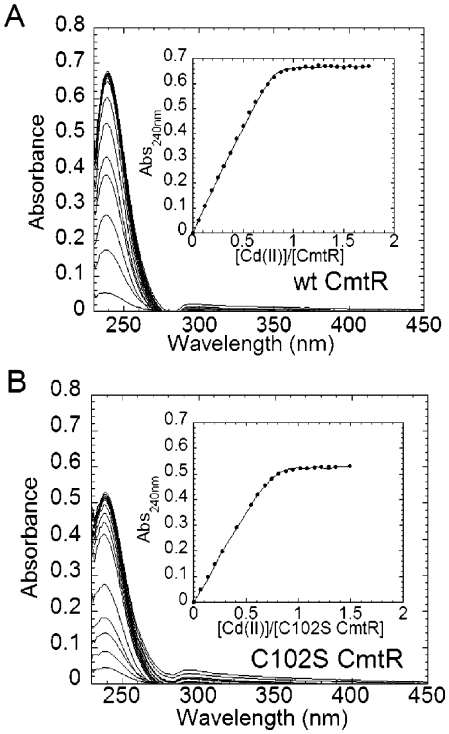

FIGURE 3: Representative anaerobic Cd^{II} titrations of (A) apo-wild-type CmtR (49.4 μM) and (B) apo-CmtR C102S CmtR (47.3 μM). (A) Full corrected ultraviolet absorption spectra that result from increasing additions of Cd^{II} are shown. (Inset) Cd^{II}-binding isotherm plotted a change in A_{240} versus [CmtR monomer]. For wild-type CmtR (A), the solid curve represents the fit to a 1:1 binding model that returns the following parameters: $K_{Cd-CmtR}$ = 9.9 (±2.3) × 10^6 M^{-1} (a lower limit under these conditions) and active [CmtR monomer] = 37.2 (±0.1) μM. For C102S CmtR (B), the solid curve defines a fit to a 1:1 binding model with $K_{Cd-CmtRC102S}$ = 3.2 (±0.4) × 10^6 M^{-1} (a lower limit) and active [C102S CmtR monomer] = 33.4 (±0.2) μM. Conditions: 10 mM HEPES and 0.4 M NaCl at pH 7.0 and 25 °C.

Nonlinear least-squares fits of the binding isotherms to a simple 1:1 metal-binding model are shown in Figure 3. This simple model was used because the Cd^{II} binding is essentially stoichiometric under these conditions and the determined stoichiometry is less than unity; however, only a lower limit for K_{Cd} can be obtained. The same experiment was therefore repeated in the presence of a large molar excess of EDTA (Figure 4), with the conditional Cd^{II}−EDTA stability constant of $K_{Cd-EDTA}$ = 3.2 × 10^{12} M^{-1} under these solution conditions. Formation of the Cd^{II}−EDTA complex is transparent under these conditions. Nonlinear least-squares fitting to a simple competition model (see the Materials and Methods) reveals that K_{Cd} for wild-type CmtR is 1.7 (±0.1) × 10^{12} M^{-1} (Figure 4A); while K_{Cd} for C102S CmtR is 1.0 (±0.1) × 10^{11} M^{-1} (Figure 4B) or nearly ≈20-fold weaker. These data collectively suggest that Cys102 affects the metal-site structure in CmtR, possibly as a weakly coordinating ligand to the Cd^{II} ion, but substitution with a nonliganding side chain reduces the stability of the Cd^{II} complex by just 10% in free energy (16.7 versus 15.0 kcal mol^{-1} for wild-type and C102S CmtR, respectively). Interestingly, K_{Cd} for CmtR is comparable to that previously determined for *S. aureus* pI258 CadC under the same solution conditions (*14*).

Pb^{II} Optical Spectroscopy. Figure 5 shows representative absorption spectra that are obtained upon anaerobic titration of Pb^{II} to ≈50 μM apo-wild-type CmtR (Figure 5A) and

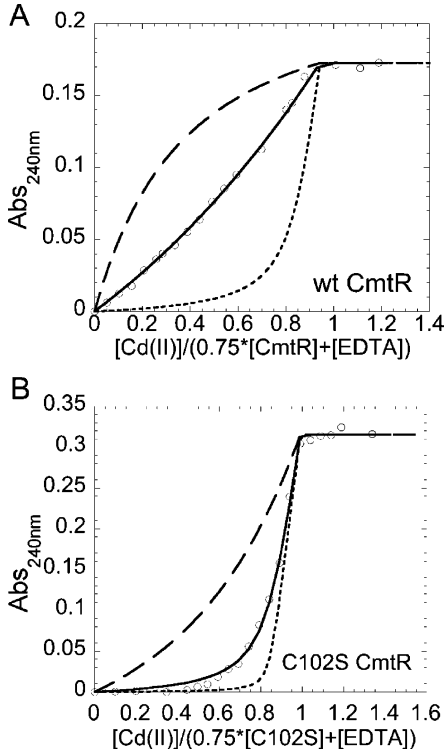

FIGURE 4: Representative Cd^{II} competition assays carried out with wild-type CmtR (19.9 μM) (A) and C102S CmtR (34 μM) in the presence of 227 μM EDTA. The Cd−EDTA complex is transparent in this assay. The solid line represents a nonlinear least-squares fit to a model that assumes one class of Cd^{II}-binding sites on the CmtR homodimer that takes into account the fractional population of active metal-binding sites (i.e., 0.75 per monomer; see Figure 3) and a conditional Cd−EDTA stability constant, $K_{Cd-EDTA}$, of 3.2×10^{12} M^{-1}. $K_{Cd-CmtR} = 1.66\ (\pm 0.04) \times 10^{12}\ M^{-1}$, $K_{Cd-CmtRC102S} = 1.03\ (\pm 0.09) \times 10^{11}\ M^{-1}$. Broken lines in each panel represent simulated curves characterized by a $K_{Cd-protein}$ of (A) $1 \times 10^{13}\ M^{-1}$ (− −) and $1 \times 10^{11}\ M^{-1}$ (- - -) and (B) $1 \times 10^{12}\ M^{-1}$ (− −) and $1 \times 10^{10}\ M^{-1}$ (- - -).

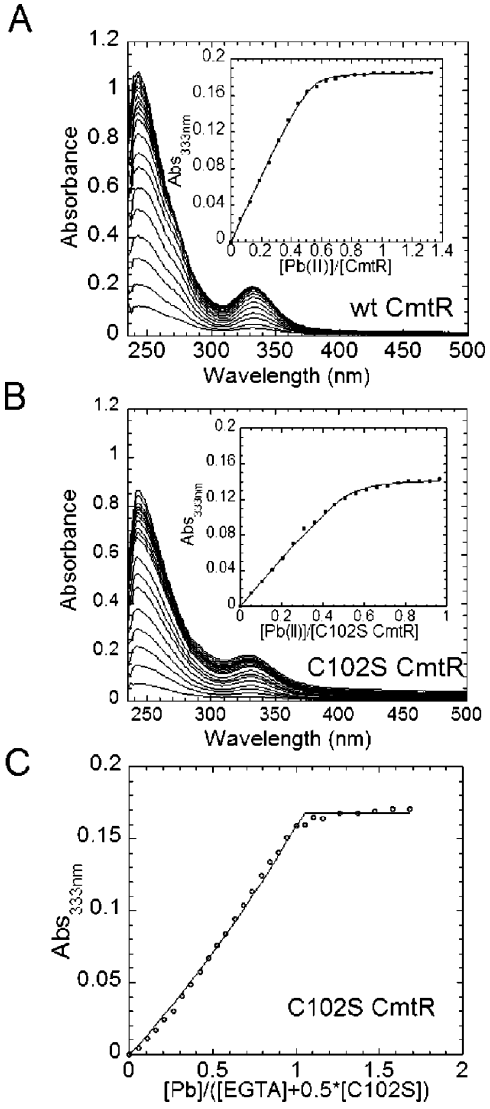

FIGURE 5: Representative anaerobic Pb^{II} titrations of (A) apo-wild-type CmtR (48.5 μM), (B) apo-C102S CmtR (56.8 μM), and (C) apo-C102S CmtR (55.1 μM) and 91.2 μM EGTA. (A) Full corrected ultraviolet absorbance spectra obtained following increasing amounts of added Pb^{II} are shown. (Inset) Pb^{II}-binding isotherm plotted a change in A_{333} versus [CmtR monomer]. For wild-type CmtR (A), the solid curve represents the fit to a 1:1 binding model that returns the following parameters: $K_{Pb-CmtR} = 4.6\ (\pm 0.6) \times 10^6\ M^{-1}$ (a lower limit) and active [CmtR monomer] = 23.3 ($\pm$0.1) μM. For C102S CmtR (B), the solid curve defines a fit to a 1:1 binding model with $K_{Pb-CmtRC102S} = 2.2\ (\pm 0.4) \times 10^6\ M^{-1}$ and active [C102S CmtR monomer] = 28.7 ($\pm$0.3) μM. Wild-type CmtR binds stronger to Pb^{II} than does EGTA (data not shown), but C102S CmtR shows a binding affinity of Pb^{II} that is comparable to EGTA (C). The solid line represents a nonlinear least-squares fit to a model that assumes one major Pb^{II}-binding sites per nondissociable CmtR dimer (i.e., 0.5 per monomer; see A) and a conditional Pb−EGTA stability constant, $K_{Pb-EGTA} = 1.38 \times 10^{10}$ M^{-1} (see the Material and Methods). $K_{Pb-C102S\ CmtR} = 8.7\ (\pm 0.4) \times 10^9\ M^{-1}$. Conditions: 10 mM bis-Tris and 0.4 M NaCl at pH 7.0 and 25 °C.

C102S CmtR (Figure 5B). As above, binding isotherms (insets) were obtained by plotting the corrected absorbance at 333 nm as a function of the $[Pb^{II}]$/[CmtR] or $[Pb^{II}]$/[C102S CmtR] ratio. The saturated Pb^{II} absorption spectra for both proteins are characterized by two distinct features: intense absorption in the far-ultraviolet and a long-wavelength absorption band with a peak maximum at 333 nm (ϵ_{333} = 7900 M^{-1} cm^{-1}), with an overall molar absorptivity again less in the C102S mutant (ϵ_{333} = 4900 M^{-1} cm^{-1}). These intense ultraviolet transitions are thought to result from a combination of S^- to Pb^{II} ligand−metal and metal−ligand charge-transfer transitions and Pb^{II} intra-atomic transitions, e.g., Pb^{II} 6s orbital to Pb^{II} 6p orbital (*38*). Unlike the case for Cd^{II}, the extent to which the absorption maximum and intensity reports on coordination number and geometry for Pb^{II}−thiolate complexes is not yet firmly established. However, in comparison to the structurally characterized $Pb^{II}-S_3$ trigonal complex of pI258 CadC, the long-wavelength absorption band of CmtR is blue-shifted relative to that of wild-type CadC and is quite similar to the S_2(O/N) complex formed by C60G CadC (*18*).

The binding titrations for wild-type CmtR (inset of Figure 5A) and C102S CmtR (inset of Figure 5B) reveal that the apparent stoichiometry of Pb^{II} binding in both cases is ≈0.5 or ≈1 per homodimer, with a $K_{Pb} \geq 10^6\ M^{-1}$ for both proteins. Chelator competition experiments such as that shown in Figure 4 with Pb^{II}−EDTA ($K_{Pb-EDTA} = 2.9 \times 10^{14}$ M^{-1}) and Pb^{II}−EGTA ($K_{Pb-EGTA} = 1.38 \times 10^{10}\ M^{-1}$) mixtures effectively bracket K_{Pb} for wild-type CmtR in the $\sim 10^{13}-10^{12}\ M^{-1}$ range (data not shown). For C102S CmtR, an EGTA−C102S CmtR competition experiment reveals a K_{Pb} comparable to that of EGTA, equal to 8.7 ($\pm$0.4) $\times 10^9$

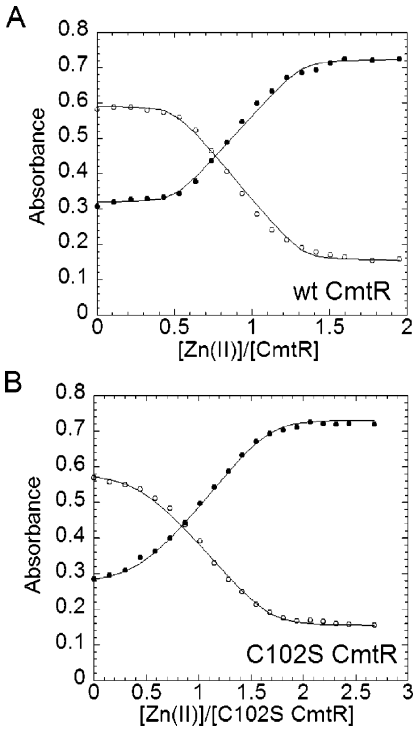

FIGURE 6: Representative titrations of Zn^{II} into a mixture of magfura-2 and either (A) wild-type CmtR or (B) C102S CmtR. (A) 22.8 μM CmtR and 18.8 μM magfura-2 and (B) 17.8 μM CmtRC102S and 19.0 μM magfura-2 were present. In both A and B, ● represents A_{325} and ○ represents A_{366}. The solid line represents a global nonlinear least-squares fit to a model that incorporates the stepwise binding of two Zn^{II} (defined by K_{ZnP_2} and $K_{Zn_2P_2}$) to a nondissociable CmtR dimer using Dynafit. For wild-type CmtR, the following parameters were obtained: $K_{ZnP_2} = 8.5\ (\pm 4.1) \times 10^9\ M^{-1}$ (a lower limit under these conditions), $K_{Zn_2P_2} = 3.0\ (\pm 1.5) \times 10^5\ M^{-1}$. For C102S CmtR, $K_{ZnP_2} = 6.5\ (\pm 1.3) \times 10^8\ M^{-1}$, $K_{Zn_2P_2} = 8.0\ (\pm 3.8) \times 10^5\ M^{-1}$. Conditions: 10 mM HEPES and 0.4 M NaCl at pH 7.0 and 25 °C.

M^{-1}, or ≈100−1000-fold weaker than wild-type CmtR (Figure 5C). The origin of the 0.5:1 Pb^{II}/CmtR monomer stoichiometry is unknown but is unlikely to be due to competition between CmtR and bis-Tris buffer, a weakly chelating buffer used to prevent $Pb(OH)_2$ precipitation during the experiment, because varying the buffer concentration (from 5 to 20 mM) had no effect on the stoichiometry (data not shown). The simplest interpretation is that there is just one high-affinity Pb^{II} site on the homodimer or, more formally, strong negative cooperativity of Pb^{II} binding where the affinity of the second Pb^{II} ion is $\leq 10^3\ M^{-1}$. Negative cooperativity of metal-ion binding has previously been previously observed for other homodimeric SmtB/ArsR metal sensors (*2*, *14*).

Zn^{II}-Binding Affinities Obtained via Chelator Competition Experiments with Magfura-2. Because previous functional experiments showed that Zn^{II} was not a strong inducer of CmtR-regulated reporter gene transcription *in vivo*, it was of interest to determine if CmtR binds Zn^{II} with high affinity. In these experiments, the well-characterized zinc indicator dye magfura-2 (K_{Zn}magfura-2 $= 5.0 \times 10^7\ M^{-1}$) was used as a competitor of Zn^{II} binding to CmtR and C102S CmtR so that the Zn^{II}-binding stoichiometry and affinity constant K_{Zn} could be determined (*21*).

Figure 6 shows representative titrations of Zn^{II} into approximately equimolar mixtures of wild-type CmtR (Figure 6A) and C102S CmtR (Figure 6B) and magfura-2. The solid curves represent a fit to a model that describes the binding of two successive Zn^{II} ions to the CmtR dimer, the affinities of which are defined by K_{ZnP_2} and $K_{Zn_2P_2}$ (see the Materials and Methods). Estimated parameters from these experiments are $K_{ZnP_2} = 8.5\ (\pm 4.1) \times 10^9\ M^{-1}$ and $K_{Zn_2P_2} = 3.0\ (\pm 1.5) \times 10^5\ M^{-1}$ for wild-type CmtR and $K_{Zn\cdot P_2} = 6.5\ (\pm 1.3) \times 10^8\ M^{-1}$ and $K_{Zn_2P_2} = 8.0\ (\pm 3.8) \times 10^5\ M^{-1}$ for C102S CmtR. K_{Zn_1} of $\approx 1 \times 10^{10}\ M^{-1}$ determined from this approach with magfura-2 provides a reasonable estimate for wild-type CmtR, because K_{Zn_1} was found to be $\approx 10^{10}\ M^{-1}$ from parallel quin-2 titrations (data not shown). As can be seen, both CmtR homodimers bind Zn^{II} with negative cooperativity, with an effective stoichiometry of tight binding sites of ≈0.5:1 or ≈1 per homodimer, with the second Zn^{II}-binding site characterized by an affinity less than magfura-2. Just like the case for strongly inducing metals Cd^{II}, the affinity of C102S CmtR for Zn^{II} is only ≈10-fold lower than wild-type CmtR but still quite tight. However, for comparison, $K_{Zn\cdot P_2}$ determined for two previously characterized Zn^{II} sensors, CzrA and SmtB, is on the order of $10^{12}-10^{14}\ M^{-1}$ (*2*, *21*); thus, CmtR binds Zn^{II} with an affinity that is weaker than other bona fide zinc sensors (see the Discussion).

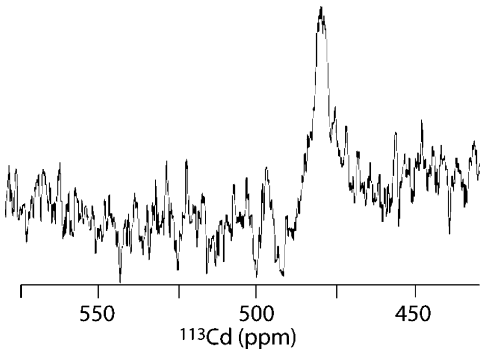

FIGURE 7: ^{113}Cd NMR spectrum of ^{113}Cd-substituted *M. tuberculosis* CmtR. Conditions: 0.8 mM ^{113}Cd-substituted CmtR in 5 mM HEPES-d_{18}, 0.35 M NaCl, and 10% D_2O at pH 7.0 and 25.0 °C. The chemical shift is reported relative to 0.10 M $Cd(ClO_4)_2$ at pH 7.0.

^{113}Cd NMR Spectroscopy of $^{113}Cd^{II}$-Bound CmtR. ^{113}Cd NMR spectroscopy of ^{113}Cd-substituted metalloproteins provides direct insight into the nature and number of coordinating atoms by virtue of magnitude of the ^{113}Cd chemical shift (δ) (*39*). In particular, thiolate ligands are more deshielding relative to other ligands, e.g., oxygen and nitrogen, and therefore induce a strongly downfield shifted chemical shift relative to aqueous $Cd(ClO_4)_2$ (*39*). ^{113}Cd-substituted wild-type CmtR shows a single broad resonance at $\delta = 480$ ppm (Figure 7). This is 132 ppm upfield of ^{113}Cd-substituted *L. monocytogenes* CadC (data not shown) and *S. aureus* pI258 CadC (*14*), each of which are characterized by three strong thiolate donor atoms. The δ for ^{113}Cd-substituted CmtR is therefore more consistent with two strong thiolate donor atoms, likely derived from Cys57 and Cys61. Repeated attempts to observe a ^{113}Cd resonance for C102S CmtR were unsuccessful under a variety of solution conditions, presumably due to chemical-exchange broadening (data not shown).

Perturbed Angular Correlation (PAC) Spectroscopy of ^{111m}Cd-Substituted CmtR and C102S CmtR. The fitted

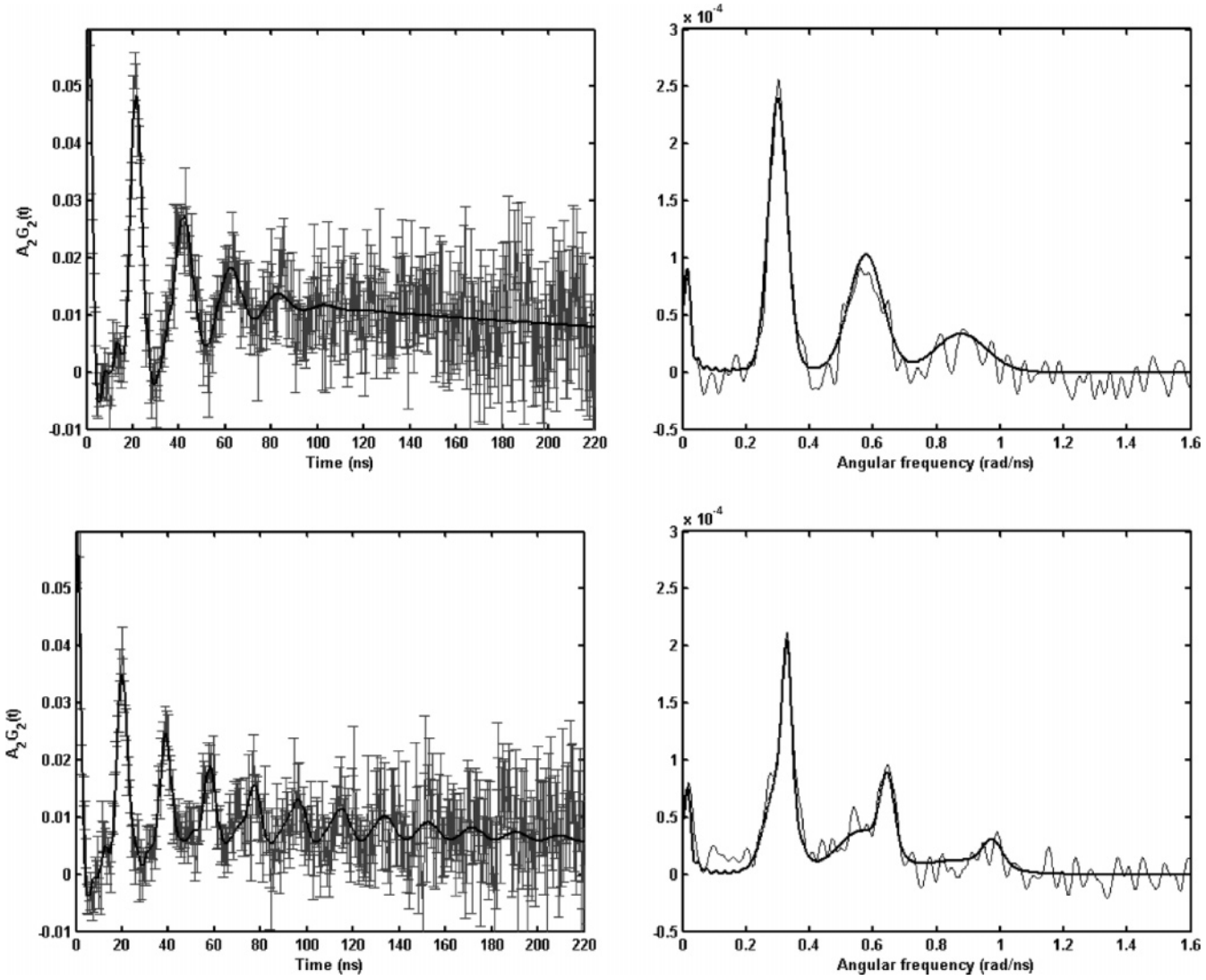

FIGURE 8: ^{111m}Cd PAC spectra of wild-type (WT) (top) and C102S (bottom) CmtRs. (Left panels) Experimentally determined perturbation function with error bars (gray) with nonlinear least-squares fit (bold-faced line) (see the Materials and Methods). (Right panels) Fourier transformations of the experimental perturbation function (thin line) and fitted function (bold-faced line). The first five points of the perturbation function are shown without their associated error bars, to indicate that they are not included in the fit. The parameters from these fits are compiled in Table 1.

Table 1: Fitted Parameters Derived from the ^{111m}Cd Perturbed Angular Correlation Spectra (see Figure 8) Obtained for Wild-Type and C102S CmtRs

protein	pH	ω_0 (rad/ns)	η	$\Delta\omega_0/\omega_0$ (×100)	τ_c (ns)	A (×100)	χ_r^2
wild type	7.0	0.291 (1)[a]	0.18 (1)	9.0 (4)	323 (42)	7.4 (3)	1.00
C102S	6.7	0.324 (1)	0.13 (2)	3.0 (5)	303 (46)	2.1 (3)	1.15
		0.285 (7)	0.27 (3)	14 (1)		3.8 (4)	

[a] The numbers in parentheses represent the standard deviation in the last digit of the fitted parameters.

experimental PAC spectra for wild-type and C102S CmtR are shown in Figure 8, with a compilation of the fitted parameters shown in Table 1. Qualitatively, the perturbation functions obtained for wild-type and C102S CmtRs are quite similar. However, a quantitative analysis of the data reveals clear differences, with the major one being that just one NQI is required to satisfactorily fit the wild-type data, whereas two NQIs are required to satisfactorily fit the C102S perturbation function (Table 1). The high-frequency spread (embodied in the $\Delta\omega_0/\omega_0$ term) of one of the two NQIs in C102S CmtR may cause the amplitude of this signal to be overestimated but is immaterial to our conclusions. All three NQIs are quite similar, and the frequencies are relatively high, indicating the presence of cysteines in the first coordination sphere. PAC parameters ω_0 and η have been calculated for selected model structures using the semiempirical BASIL method and are compiled in Table 2 (*40*). A comparison of the observed ω_0 and η for wild-type and C102S CmtRs with those derived from model complexes reveals that a trigonal pyramidal coordination geometry with three coordinating cysteines and distorted tetrahedral coordination geometries of the Cys_3-H_2O or $Cys_2-(H_2O)_2$ type are all consistent with the experimental data. The values of ω_0 (Tables 1 and 2) reveal that both tetrahedral Cys_4 and trigonal planar Cys_3 cadmium structures compare very unfavorably with the data (*26*, *37*). However, there are coordination complexes that are not adequately described by this semiempirical model (*41*).

The qualitative similarity of the spectra for the wild-type and C102S CmtRs suggest that Cys102, if coordinated, has only a weak interaction with the cadmium ion in the free

Table 2: Calculated PAC Parameters for Model Coordination Complexes Derived from the Semiempirical BASIL Method (*40*)

coordination sphere	model structure	ω_0 (rad/ns)	η
$[Cd(Cys)_4]^{-2}$	tetrahedral	0.000	not defined
$[Cd(Cys)_3]^{-1}$	trigonal planar	0.450	0.00
$[Cd(Cys)_3]^{-1}$	trigonal pyramidal	0.300	0.00
$[Cd(Cys)_3H_2O]^{-1}$	tetrahedral	0.093	0.00
$[Cd(Cys)_3H_2O]^{-1}$	distorted tetrahedral[a]	0.261	0.23
$[Cd(Cys)_2(H_2O)_2]$	tetrahedral	0.093	1.00
$[Cd(Cys)_2(H_2O)_2]$	distorted tetrahedral[b]	0.276	0.33

[a] The S−Cd−S angle increased from 109.47° to 125° for two of the cysteines. [b] The S−Cd−S angle increased from 109.47° to 135°.

protein. Thus, a complex formed by Cys57, Cys61, and possibly Cys102 as a weakly bound ligand and another nonthiolate protein-derived ligand or molecule from the solvent (Cl^- or H_2O) seems most consistent with all the data (see the Discussion). Clearly however, substitution of Cys102 with Ser increases the heterogeneity of the metal coordination sphere with two or more structurally distinct complexes, indicating a role for Cys102 is stabilization of the metal-binding site structure in wild-type CmtR (Figures 4−6). The fact that two coordination geometries are detected by PAC spectroscopy for C102S CmtR demonstrates that they are in slow exchange on the PAC time scale (ns). However, they may be in intermediate exchange on the ^{113}Cd NMR time scale ($\approx\mu$s), and this could explain our inability to observe a ^{113}Cd resonance for C102S CmtR (*vide supra*). The relatively low values of η obtained for all metal structures (Table 1) are indicative of coordination geometries only slightly distorted from axial symmetry.

Allosteric Negative Regulation of cmt O/P Binding by Cd^{II} Ions. Previously published gel-mobility shift experiments proposed that a 10−5−10 hyphenated inverted repeat in the *cmt* O/P is the regulatory binding site for CmtR (*1*). However, these data provided no information on the CmtR−DNA-binding stoichiometry or affinity in the presence and absence of bound metal ions. We therefore designed a fluorescein-labeled 40 base pair duplex oligonucleotide that encompasses the full imperfect 10−5−10 repeat (*1*) and monitored the binding of wild-type and C102S CmtRs by measuring changes in the anisotropy of the fluorescein fluorescence of the labeled DNA (*12*, *14*, *15*, *18*, *34*).

Figure 9 shows representative binding isotherms obtained for wild-type CmtR (Figure 9A) and C102S CmtR (Figure 9B) in the presence (10 μM $CdCl_2$) and absence (50 μM EDTA) of saturating Cd^{II} at pH 7.0, 0.40 M NaCl, and 25 °C, with solution conditions identical to the analytical ultracentrifugation and metal-binding experiments described above. The solid line through each data set represents nonlinear least-squares fit to a sequential dimer binding model (see the Materials and Methods), with the results from multiple experiments compiled in Table 3. The magnitude of the change in anisotropy reveals that both CmtR and C102S CmtR oligomerize on the DNA and form 1:1, 2:1, and 3:1 protein dimer−DNA complexes, similar to that previously observed for CzrA and SmtB (*12*, *34*). The binding affinities obtained for apo-CmtR are $K_1 = 7.9\ (\pm 1.8) \times 10^6\ M^{-1}$, $K_2 = 1.3\ (\pm 0.2) \times 10^6\ M^{-1}$, and $K_3 = 4.5\ (\pm 0.5) \times 10^5\ M^{-1}$ (Figure 9A and Table 3). Although these values reflect relatively weak DNA-binding affinity relative to CadC

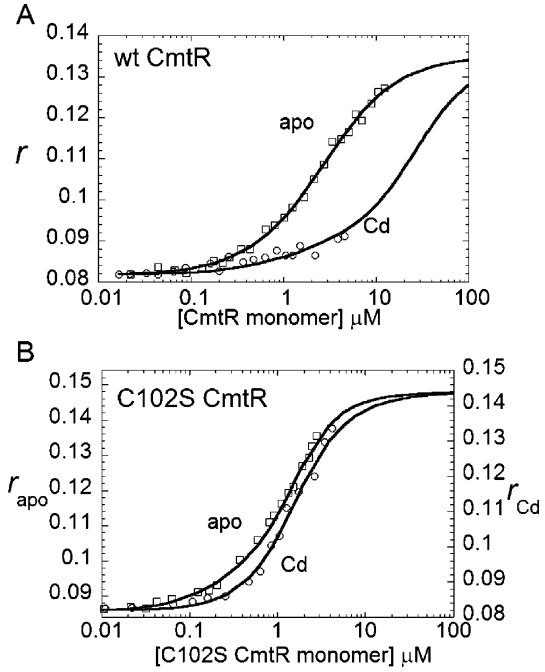

FIGURE 9: Representative *cmt* O/P binding by wild-type (A) and C102S CmtR (B) as monitored by fluorescence anisotropy. A 40-bp 5′-fluorescein-labeled oligonucleotide containing the *cmt* O/P was used for these experiments. Conditions: 10 mM HEPES, 0.4 M NaCl, 1 mM DTT, and 50 μM EDTA (for apoprotein titrations) (□) or 10 μM Cd^{II} (in Cd−CmtR titrations) (○) at pH 7.0. The solid line through each set of data represents the best fit of anisotropy data to a dissociable dimer model assuming a 3:1 dimer/DNA complex with K_{dimer} fixed at $1.7 \times 10^7\ M^{-1}$ for wild-type CmtR and C102S CmtR. The following parameters were obtained: (A) apo-wild-type CmtR, $K_1 = 7.9\ (\pm 1.8) \times 10^6\ M^{-1}$, $K_2 = 1.3\ (\pm 0.2) \times 10^6\ M^{-1}$, and $K_3 = 4.5\ (\pm 0.5) \times 10^5\ M^{-1}$; Cd−CmtR, $K_1 = 1.6\ (\pm 0.3) \times 10^6\ M^{-1}$ and $K_2 = K_3 \leq 8 \times 10^4\ M^{-1}$ (upper limit); (B) apo-C102S CmtR, $K_1 = 1.2\ (\pm 0.2) \times 10^7\ M^{-1}$, $K_2 = 0.9\ (\pm 0.3) \times 10^6\ M^{-1}$, and $K_3 = 2.6\ (\pm 0.7) \times 10^6\ M^{-1}$; Cd−C102S CmtR, $K_1 = 2.7\ (\pm 1.1) \times 10^6\ M^{-1}$, $K_2 = 1.7\ (\pm 0.9) \times 10^6\ M^{-1}$, and $K_3 = 1.2\ (\pm 0.4) \times 10^6\ M^{-1}$.

under the same solution conditions (*12*, *14*), the binding is specific because CmtR shows no binding to the *nmt* O/P DNA fragment up to a monomer concentration of 10 μM (data not shown). Furthermore, Cd^{II} negatively allosterically regulates wild-type CmtR *cmt* O/P binding, reducing the binding affinity of the first dimer by ≈5-fold, $K_1 = 1.6\ (\pm 0.3) \times 10^6\ M^{-1}$, while eliminating detectable formation of the 2:1 and 3:1 protein−DNA complexes up to 10 μM monomer concentration (K_2 and $K_3 \leq 8 \times 10^4\ M^{-1}$).

As expected, apo-C102S CmtR behaves much like apo-wild-type CmtR and is characterized by *cm*t O/P binding affinities of $K_1 = 1.2\ (\pm 0.2) \times 10^7\ M^{-1}$, $K_2 = 0.9\ (\pm 0.3) \times 10^6\ M^{-1}$, and $K_3 = 2.6\ (\pm 0.7) \times 10^6\ M^{-1}$ (Figure 9B and Table 3). In contrast, the binding isotherm for Cd^{II}-saturated C102S CmtR is different from that of Cd^{II}-substituted wild-type CmtR (Figure 9A), with Cd^{II}-bound C102S CmtR still capable of forming 1:1, 2:1, and 3:1 complexes. Resolution of the binding parameters gives $K_1 = 2.7\ (\pm 1.1) \times 10^6\ M^{-1}$, $K_2 = 1.7\ (\pm 0.9) \times 10^6\ M^{-1}$, and $K_3 = 1.2\ (\pm 0.4) \times 10^6\ M^{-1}$. These findings reveal that Cd^{II} is fully capable of allosterically negatively regulating the binding of the first C102S CmtR homodimer to DNA to an extent indistinguishable from wild-type CmtR ($\Delta G_c \approx 1.0$ kcal mol^{-1}) (Table 3). In contrast, Cd^{II} has little effect on the formation of higher order complexes formed by C102S CmtR on the DNA

Table 3: Summary of K_i Obtained for the Binding of Apo, Cd-Substituted, and Zn^{II}-Substituted Wild-Type and C102S CmtR to *cmt* O/P DNA[a]

		K_1 ($\times 10^6\,M^{-1}$)	K_2 ($\times 10^6\,M^{-1}$)	K_3 ($\times 10^6\,M^{-1}$)	ΔG_1[b] (kcal mol^{-1})	$\sum\Delta G$ (kcal mol^{-1})	ΔG_c[c] (kcal mol^{-1})	$\Delta G_c^{\Sigma G}$[d] (kcal mol^{-1})
CmtR	apo	6.8 ± 1.9	1.4 ± 0.3	0.6 ± 0.1	-9.3	-25.5		
	Cd	1.4 ± 0.3	≤ 0.08	≤ 0.08	-8.3	-21.7	1.0	≥ 3.8
	Zn	1.0 ± 0.2	≤ 0.08	≤ 0.08	-8.1	-21.4	1.2	≥ 4.1
C102S CmtR	apo	11.1 ± 1.9	1.2 ± 0.4	2.2 ± 0.5	-9.6	-26.4		
	Cd	3.0 ± 0.9	1.6 ± 0.8	1.1 ± 0.3	-8.8	-25.4	0.8	1.0
	Zn	2.1 ± 0.7	0.4 ± 0.2	1.0 ± 0.4	-8.6	-24.3	1.0	2.1

[a] K_i reflects the mean of $K_i \pm$ standard error determined from 2 to 3 independent experiments. [b] $\Delta G_1 = -RT \ln K$ ($T = 298$ K). [c] $\Delta G_c = \Delta G_{1\ \mathrm{metal}} - \Delta G_{1\ \mathrm{apo}}$. [d] $\Delta G_c^{\Sigma G} = \sum\Delta G_{\mathrm{metal}} - \sum\Delta G_{\mathrm{apo}}$.

(compare the last two columns of Table 3). The same trends in allostery are also observed with Zn^{II} (Table 3) and Pb^{II} (data not shown). These results show that Cys102 functions as a key regulatory metal ligand, consistent with *in vivo* experiments that showed that C102S CmtR-regulated reporter gene expression is unresponsive to Cd^{II} addition (*1*). However, they reveal that C102S CmtR is refractory to the metal-mediated disassembly of 2:1 and 3:1 CmtR homodimer/DNA higher order complexes, rather than at the first dimer-binding step as observed for other SmtB/ArsR metalloregulators (*12*, *14*, *34*). They further argue that the minimal functional repressing complex *in vivo* is a 2:1 CmtR dimer/DNA complex.

DISCUSSION

Multiple Sequence Alignment with Other SmtB/ArsR Family Proteins. The Cavet and Robinson groups (*1*) previously established that *M. tuberculosis* CmtR contained Cd^{II}/Pb^{II}-sensing sites that must be structurally distinct from previously well-characterized α3N and α5 sites in SmtB/ArsR sensors. A multiple sequence alignment (Figure 1B) shows that *M. tuberculosis* CmtR (*1*), a previously characterized Hg^{II} sensor *S. lividans* MerR (*25*), and putative homologues in other actinomycytes have just three conserved Cys, corresponding to Cys57, Cys61, and Cys102 in *M. tuberculosis* CmtR, and completely lack the cysteine residues that comprise the well-characterized α3N Cd^{II}/Pb^{II}-sensing sites found in CadCs (*14*, *15*, *17*, *18*). Indeed, we have recently purified a CmtR homologue from *Streptomyces coelicolor* A3(2) (NP_627722) (see Figure 1B) and have shown that the Pb^{II} absorption spectrum is indistinguishable from that of *M. tuberculosis* CmtR.[3] How do the Cd^{II}- and Pb^{II}-binding properties of these two classes of heavy-metal sensing sites compare?

Comparative Metal-Binding Properties of CmtR and pI258 CadC. In general, the binding of the first Cd^{II} or Pb^{II} ion to the CmtR homodimer occurs with an affinity that is within an order of magnitude of K_{Cd} and K_{Pb} for CadC (*14*). The greatest difference has to do with the extent of apparent negative cooperativity of metal binding, which appears to be far greater for CmtR versus CadC (*14*); in fact, binding of a second Pb^{II} ion to the CmtR homodimer could not be observed under these experimental conditions (Figure 5), a finding formally consistent with "half-the-sites reactivity" (*42*−*44*). Interestingly, the Hg^{II} regulator, MerR, binds a single Hg^{II} ion per dimer (*45*), and this is sufficient to allosterically induce underwinding/bending (*46*) of the *mer* operator/promoter. Likewise, a single Pb^{II} ion per CmtR dimer appears necessary and sufficient to allosterically regulate *cmt* O/P binding to the full extent (Figure 9).[4] This is in contrast to what has been reported for CadC (*47*).

The first coordination shells of CadC and CmtR are clearly different as well. Previous spectroscopic studies of CadC are consistent with a strongly distorted S_4 or S_3O Cd^{II} complex and a trigonal S_3 Pb^{II} complex (*14*, *18*). The Cd^{II} and Pb^{II} chelates of CmtR are generally indicative of lower molar absorptivities and, in the case of the Pb^{II} spectrum, a significant blue-shift, relative to the Cd^{II} and Pb^{II} complexes formed by CadC (*14*, *18*). These data collectively suggest that CmtR has one fewer strongly bound thiolate ligand, a result consistent with the ^{113}Cd NMR resonance frequencies obtained for CmtR ($\delta = 480$ ppm) versus CadC ($\delta = 622$ ppm) (*14*). This result alone would seem to rule out direct metal coordination by Cys102 in the free protein, although the Cd^{II} optical titrations and a comparison of the K_{Me} for wild-type and C102S CmtRs (Figures 3−5) would seem to argue against this. Cys102 might be analogous to Cys11 in *S. aureus* pI258 CadC, which has been argued to be a weakly bound or weakly deshielding (of the ^{113}Cd nucleus) thiol(ate) ligand (*18*, *48*), perhaps because of a longer than normal coordination bond, a proposal supported by recent theoretical calculations (*39*). In contrast to Cys11 in CadC however, Cys102 in CmtR is a key allosteric metal ligand (*vide infra*).

It is noteworthy that a relatively high frequency (ω_0) characterizes the PAC spectrum of $^{111m}Cd^{II}$-substituted wild-type CmtR (Figure 8 and Table 1). This feature distinguishes CmtR from CadC. CadC adopts a distorted tetrahedral complex that is expected to give a much lower ω_0, as measured, for example, for the tetrathiolate structural metal-ion-binding site in horse liver alcohol dehydrogenase (*32*); recent PAC experiments of ^{111m}Cd-substituted CadC are consistent with this interpretation (L. Busenlehner, X. Chen, L. Hemmingsen, M. K. Jensen, R. Bauer, and D. Giedroc, manuscript in preparation).[5] PAC spectroscopy of wild-type versus C102S CmtR does not unambiguously reveal if Cys102 is a first shell ligand in the free protein because both spectra are quite similar; however, substitution of Cys102 with a nonliganding Ser side chain clearly increases the structural heterogeneity of the metal complex. Pb^{II} EXAFS, like that previously done for CadC (*18*), will be required to unambiguously determine the number of thiolate donor atoms in the Pb^{II} coordination complexes of Pb^{II}-substituted wild-

[3] Y. Wang and D. Giedroc, unpublished observations.

[4] Characterization of covalently fused dimers of a related SmtB/ArsR Zn^{II}/Co^{II} sensor CzrA (*2*) reveal that metal binding to just one of the two identical sites on the dimer mediates significant allosteric regulation of O/P binding (S. Lee, M. Shubina, and D. Giedroc, manuscript in preparation).

[5] L. Busenlehner, Ph.D. dissertation, Texas A&M University.

type and C102S CmtR. It is worth noting that the Co^{II} UV−vis absorption spectrum of Co^{II}-CmtR is quite unusual (*1*) (data not shown) but similar (albeit slightly blue-shifted), to that of *L. monocytogenes* CadC (*18*), with at least three well-resolved low intensity ligand-field transitions ($\lambda = 530$, 675, and 760 nm); this spectrum suggests a strongly distorted Co^{II} complex.

Although the biological data are limited, some CadCs mediate metalloregulation of gene expression by Zn^{II} in addition to more thiophilic ions Cd^{II} and Pb^{II}; in the case of *S. aureus* pI258 CadC, zinc resistance via derepression of the *cad* operon (which encodes genes for both CadC and CadA, a P-type ATPase) is robust in *E. coli* that lack the major zinc-resistance system encoded by the *znt* operon (*23*). Interestingly, induction of the *cmt* operon in *M. smegmatis* is reported to be selective for Cd^{II} and Pb^{II}, with no induction mediated by Zn^{II}, at least at the concentrations tested (*1*). Our original thought was that perhaps CmtR bound Zn^{II} weakly by virtue of forming a lower coordination number ($n = 3$) complex, because Zn^{II} shows a strong preference for four-coordinate complexes or higher. This proved not to be the case, because the binding affinity of the first Zn^{II} to CmtR is quite high ($K_{Zn_1} \approx 10^{10}$ M^{-1}) (Figure 6). Nonetheless, this is lower than the estimates of K_{Zn} for pI258 CadC by at least an order of magnitude[5] and far lower than that determined for bona fide SmtB/ArsR Zn^{II} sensors SmtB (*11*, *21*) and CzrA (*2*). In any case, Zn^{II} is an effective allosteric regulator of CmtR−*cmt* O/P binding equilibria *in vitro* (Figure 9) and is in fact indistinguishable from Cd^{II} and Pb^{II} in this assay. Previous studies with other SmtB/ArsR sensors reveal that coordination geometry is a major determinant for metal selectivity (*12*) (M. Pennella and D. Giedroc, submitted for publication); thus, Zn^{II} may adopt a metal complex that is isostructural with that of the Pb^{II} and Cd^{II} complexes.

Why then is Zn^{II} a noninducer *in vivo*? One possibility is that Zn^{II} fluxes in *M. smegmatis* simply do not reach the levels sufficient to induce the *cmt* operon *in vivo*, relative to toxic heavy metals Cd^{II} and Pb^{II}. Alternatively, there are differences in the extent to which biologically essential Zn^{II} is trafficked or made bioavailable in *M. smegmatis*. Indeed, previous work from the Robinson laboratory reveals that *M. smegmatis* does not accumulate Zn^{II} when cultured in media containing maximally permissive concentrations of Zn^{II} salts (*20*); thus, it is not surprising that CmtR does not sense Zn^{II} in *M. smegmatis*. It would be of interest to determine if *cmt* expression could be induced in a cyanobacterial cell, where Zn^{II} pools are clearly sufficient to be detected by known high-affinity zinc sensor, *Synechococcus* SmtB (*20*). These findings also partly explain why Zn^{II} is a noninducer of the Ni^{II}/Co^{II}-responsive *nmt* operon in *M. smegmatis*, which encodes the Ni^{II}/Co^{II}-sensing SmtB/ArsR repressor, NmtR (*20*); however, in this case, Zn^{II} is a poorer allosteric inducer *in vitro* as well, relative to Ni^{II} and Co^{II}, because it fails to adopt the proper coordination geometry in the regulatory metal sites (*12*).

How Do Metal Ions Induce Negative Allosteric Regulation of CmtR Binding to the cmt O/P? Quantitative fluorescence anisotropy-based DNA-binding experiments analyzed with a multiple-dimer-binding model reveal that all metal ions tested, Cd^{II}, Pb^{II}, and Zn^{II}, lower the binding affinity of all CmtR homodimers for the *cmt* O/P, with the effect greatest on the formation of higher order (2:1 and 3:1) complexes, which are not observed under these conditions (Figure 9 and Table 3). Stated another way, inducing metals regulate the assembly state by mediating the disassembly of an oligomeric protein−DNA complex. Strikingly, substitution of Cys102 with a nonliganding Ser essentially abrogates metalloregulation of the assembly of 2:1 and 3:1 complexes, with little influence on the binding of the first dimer. These features are novel relative to other SmtB/ArsR family metalloregulators, where the binding of inducing metal ions lowers the affinity of the first dimer by 300−10 000-fold, giving an allosteric coupling free energy, ΔG_c of $\approx +3$ to $\geq +5$ kcal mol^{-1} (25 °C) (*12*, *14*, *34*) (M. Pennella and D. Giedroc, submitted for publication). In the case of CmtR, ΔG_c is small, ≤ 1.0 kcal mol^{-1}, and is not appreciably affected by substitution of this key allosteric ligand (Table 3). One intriguing possibility is that the C-terminal Cys102 (see Figure 1A) mediates the formation of metal-cross-linked tetramers on the DNA, with Cys102 from one dimer forming a metal coordination bond to the opposite dimer, with formation of this metal-liganded tetramer significantly lowering CmtR-binding affinity. This exciting possibility remains to be tested. In any case, Cys102 in CmtR is functionally analogous to allosteric ligands Cys7 and Cys60 in *S. aureus* pI258 CadC, mutagenesis of which significantly reduces (Cys7) or completely abrogates (Cys60) Cd^{II}/Pb^{II}-mediated metalloregulation of *cad* O/P binding (*18*).

When our data are taken together, they suggest a "division of labor" within the metal-sensing chelate of CmtR. Cys57 and Cys61, at the C terminus of the proposed α4 helix (Figure 1A), anchor the metal coordination complex; replacement of either of these two residues with nonliganding residues is expected to greatly diminish metal-binding affinity, consistent with the lack of a metal response for C57S and C61S CmtRs *in vivo* (*1*). Remarkably, metal binding to the Cys57/Cys61 pair in CmtR occurs in exactly the same region of the protein that is coupled to the interhelical α5 Zn^{II} sites in the zinc sensors SmtB and CzrA, via an intersubunit hydrogen-bonding network (*2*). However, metal coordination by the Cys57/Cys61 pair is necessary but not sufficient because Cys102, while playing a comparatively minor role in stabilizing the chelate in the uncomplexed protein, is required to fully mediate allosteric coupling of metal and *cmt* O/P binding (Figure 9); this explains the inducer nonresponsiveness of C102S CmtR in *M. smegmatis* (*1*).

Possible Biological Function of CmtR. The biological function of CmtR in *M. tuberculosis* is not yet known. However, CmtA exhibits very high sequence similarity to the well-characterized P_{1B}-type heavy-metal transporting ATPases from *E. coli* (ZntA) as well as *S. aureus* (CadA). *E. coli* ZntA is capable of effluxing Cd^{II}, Pb^{II}, and Zn^{II} (*23*, *24*, *49*, *50*), and its expression is metalloregulated by the MerR family regulator ZntR (*51*). Although Zn^{II} was the first metal-ion inducer identified for ZntA (*51*), Cd^{II} and Pb^{II} were subsequently shown to upregulate *ZntA* expression as well (*50*); in fact, one analysis of the metal inducibility profile of *zntA-lacZ* fusion constructs revealed that Cd^{II} was the most potent inducer, relative to Zn^{II} and Pb^{II} in *E. coli* (*50*). A similar metal specificity profile appears to characterize *S. aureus* CadA as well, whose expression is regulated by the SmtB/ArsR family regulator CadC in response to Cd^{II}, Pb^{II}, and to a lesser extent Zn^{II} (*52*). This leads us to propose

that *M. tuberculosis* CmtA will have similar metal-exporting properties as ZntA and CadA. Why *M. tuberculosis* encodes the *cmt* operon is unknown, because this opportunistic pathogen is unlikely to encounter Cd^{II}/Pb^{II} toxicity during the course of its life cycle. It remains to be determined whether this operon is regulated by other stress responses *in vivo*.

Finally, it is striking to note that three distinct metalloregulators, the MerR family regulator ZntR, and two structurally distinct SmtB/ArsR regulators CadC and CmtR, all regulate the expression of what appears to be essentially the same P-type ATPase efflux pump in response to the same overlapping set of divalent metal ions. This suggests a "mix and match" approach in the evolution of heavy-metal resistance systems (sensor plus resistance genes) of defined metal selectivities, perhaps mediated by the recently documented lateral transfer of genes encoding P_{IB}-type ATPase efflux pumps among subsurface bacterial species (*53*).

ACKNOWLEDGMENT

We gratefully acknowledge the help of Drs. Mario Pennella and Xiaohua Chen in preparing the ^{113}Cd-CmtR samples and Mr. Peter Cornish and Dr. Xiangming Kong in acquiring the ^{113}Cd NMR data.

NOTE ADDED AFTER ASAP PUBLICATION

This paper was originally published June 4, 2005 with an incorrect entry in Table 2. The correct version was published June 6, 2005.

REFERENCES

1. Cavet, J. S., Graham, A. I., Meng, W., and Robinson, N. J. (2003) A cadmium−lead-sensing ArsR−SmtB repressor with novel sensory sites. Complementary metal discrimination by NmtR and CmtR in a common cytosol, *J. Biol. Chem. 278*, 44560−44566.
2. Eicken, C., Pennella, M. A., Chen, X., Koshlap, K. M., VanZile, M. L., Sacchettini, J. C., and Giedroc, D. P. (2003) A metal−ligand-mediated intersubunit allosteric switch in related SmtB/ArsR zinc sensor proteins, *J. Mol. Biol. 333*, 683−695.
3. Finney, L. A., and O'Halloran, T. V. (2003) Transition metal speciation in the cell: Insights from the chemistry of metal ion receptors, *Science 300*, 931−936.
4. Wunderli-Ye, H., and Solioz, M. (1999) Copper homeostasis in *Enterococcus hirae*, *Adv. Exp. Med. Biol. 448*, 255−264.
5. Outten, C. E., and O'Halloran, T. V. (2001) Femtomolar sensitivity of metalloregulatory proteins controlling zinc homeostasis, *Science 292*, 2488−2492.
6. Rosen, B. P. (1996) Bacterial resistance to heavy metals and metalloids, *J. Biol. Inorg. Chem. 1*, 273−277.
7. Busenlehner, L. S., Pennella, M. A., and Giedroc, D. P. (2003) The SmtB/ArsR family of metalloregulatory transcriptional repressors: Structural insights into prokaryotic metal resistance, *FEMS Microbiol. Rev. 27*, 131−143.
8. Brown, N. L., Stoyanov, J. V., Kidd, S. P., and Hobman, J. L. (2003) The MerR family of transcriptional regulators, *FEMS Microbiol. Rev. 27*, 145−163.
9. Robinson, N. J., Whitehall, S. K., and Cavet, J. S. (2001) Microbial metallothioneins, *Adv. Microb. Physiol. 44*, 183−213.
10. Ralston, D. M., and O'Halloran, T. V. (1990) Ultrasensitivity and heavy-metal selectivity of the allosterically modulated MerR transcription complex, *Proc. Natl. Acad. Sci. U.S.A. 87*, 3846−3850.
11. VanZile, M. L., Cosper, N. J., Scott, R. A., and Giedroc, D. P. (2000) The zinc metalloregulatory protein *Synechococcus* PCC7942 SmtB binds a single zinc ion per monomer with high affinity in a tetrahedral coordination geometry, *Biochemistry 39*, 11818−11829.
12. Pennella, M. A., Shokes, J. E., Cosper, N. J., Scott, R. A., and Giedroc, D. P. (2003) Structural elements of metal selectivity in metal sensor proteins, *Proc. Natl. Acad. Sci. U.S.A. 100*, 3713−3718.
13. Liu, T., Nakashima, S., Hirose, K., Shibasaka, M., Katsuhara, M., Ezaki, B., Giedroc, D. P., and Kasamo, K. (2004) A novel cyanobacterial SmtB/ArsR family repressor regulates the expression of a CPx-ATPase and a metallothionein in response to both Cu^{I}/Ag^{I} and Zn^{II}/Cd^{II}. *J. Biol. Chem. 279*, 17810−17818.
14. Busenlehner, L. S., Cosper, N. J., Scott, R. A., Rosen, B. P., Wong, M. D., and Giedroc, D. P. (2001) Spectroscopic properties of the metalloregulatory Cd^{II} and Pb^{II} sites of *S. aureus* pI258 CadC, *Biochemistry 40*, 4426−4436.
15. Busenlehner, L. S., Apuy, J. L., and Giedroc, D. P. (2002) Characterization of a metalloregulatory bismuth(III) site in *Staphylococcus aureus* pI258 CadC repressor, *J. Biol. Inorg. Chem. 7*, 551−559.
16. Ji, G., and Silver, S. (1992) Regulation and expression of the arsenic resistance operon from *Staphylococcus aureus* plasmid pI258, *J. Bacteriol. 174*, 3684−3694.
17. Endo, G., and Silver, S. (1995) CadC, the transcriptional regulatory protein of the cadmium resistance system of *Staphylococcus aureus* plasmid pI258, *J. Bacteriol. 177*, 4437−4441.
18. Busenlehner, L. S., Weng, T. C., Penner-Hahn, J. E., and Giedroc, D. P. (2002) Elucidation of primary (α3N) and vestigial (α5) heavy metal-binding sites in *Staphylococcus aureus* pI258 CadC: Evolutionary implications for metal ion selectivity of ArsR/SmtB metal sensor proteins, *J. Mol. Biol. 319*, 685−701.
19. Shi, W., Wu, J., and Rosen, B. P. (1994) Identification of a putative metal binding site in a new family of metalloregulatory proteins, *J. Biol. Chem. 269*, 19826−19829.
20. Cavet, J. S., Meng, W., Pennella, M. A., Appelhoff, R. J., Giedroc, D. P., and Robinson, N. J. (2002) A nickel−cobalt-sensing ArsR−SmtB family repressor. Contributions of cytosol and effector binding sites to metal selectivity, *J. Biol. Chem. 277*, 38441−38448.
21. VanZile, M. L., Chen, X., and Giedroc, D. P. (2002) Structural characterization of distinct α3N and α5 metal sites in the cyanobacterial zinc sensor SmtB, *Biochemistry 41*, 9765−9775.
22. Cook, W. J., Kar, S. R., Taylor, K. B., and Hall, L. M. (1998) Crystal structure of the cyanobacterial metallothionein repressor SmtB: A model for metalloregulatory proteins, *J. Mol. Biol. 275*, 337−346.
23. Rensing, C., Sun, Y., Mitra, B., and Rosen, B. P. (1998) Pb^{II}-translocating P-type ATPases, *J. Biol. Chem. 273*, 32614−32617.
24. Rensing, C., Mitra, B., and Rosen, B. P. (1997) The *zntA* gene of *Escherichia coli* encodes a Zn^{II}-translocating P-type ATPase, *Proc. Natl. Acad. Sci. U.S.A. 94*, 14326−14331.
25. Rother, D., Mattes, R., and Altenbuchner, J. (1999) Purification and characterization of MerR, the regulator of the broad-spectrum mercury resistance genes in *Streptomyces lividans* 1326, *Mol. Gen. Genet. 262*, 154−162.
26. Hemmingsen, L., Sas, K. N., and Danielsen, E. (2004) Biological applications of perturbed angular correlations of γ-ray spectroscopy, *Chem. Rev. 104*, 4027−4062.
27. Pace, C. N., Vajdos, F., Fee, L., Grimsley, G., and Gray, T. (1995) How to measure and predict the molar absorption coefficient of a protein, *Protein Sci. 4*, 2411−2423.
28. Guo, J., and Giedroc, D. P. (1997) Zinc site redesign in T4 gene 32 protein: Structure and stability of cobalt(II) complexes formed by wild-type and metal ligand substitution mutants, *Biochemistry 36*, 730−742.
29. Payne, J. C. ter Horst, M. A.; Godwin, H. A. (1999) Lead fingers: Pb^{2+} binding to structural zinc-binding domains determined directly by monitoring lead−thiolate charge-transfer bands, *J. Am. Chem. Soc. 121*, 6850−6855.
30. Martell, A. E., and Smith R. M. (1974−1989) *Critical Stability Constants*, Plenum Press, New York.
31. Nasir, M. S., Fahrni, C. J., Suhy, D. A., Kolodsick, K. J., Singer, C. P., and O'Halloran, T. V. (1999) The chemical cell biology of zinc: Structure and intracellular fluorescence of a zinc−quinolinesulfonamide complex, *J. Biol. Inorg. Chem. 4*, 775−783.
32. Hemmingsen, L., Bauer, R., Bjerrum, M. J., Zeppezauer, M., Adolph, H. W., Formicka, G., and Cedergren-Zeppezauer, E. (1995) Cd-substituted horse liver alcohol dehydrogenase: Catalytic site metal coordination geometry and protein conformation, *Biochemistry 34*, 7145−7153.

33. Frauenfelder, H., Steffen, R. M. (1965) α-, *β- and γ-Ray Spectroscopy* (Siegbahn, K., Ed.), North-Holland: Amsterdam, The Netherlands, pp 997−1198.
34. VanZile, M. L., Chen, X., and Giedroc, D. P. (2002) Allosteric negative regulation of *smt* O/P binding of the zinc sensor, SmtB, by metal ions: A coupled equilibrium analysis, *Biochemistry 41*, 9776−9786.
35. Pountney, D. L., Tiwari, R. P., and Egan, J. B. (1997) Metal- and DNA-binding properties and mutational analysis of the transcription activating factor, B, of coliphage 186: A prokaryotic C4 zinc-finger protein, *Protein Sci. 6*, 892−902.
36. Henehan, C. J., Pountney, D. L., Zerbe, O., and Vasak, M. (1993) Identification of cysteine ligands in metalloproteins using optical and NMR spectroscopy: Cadmium-substituted rubredoxin as a model [Cd(CysS)4]2- center, *Protein Sci. 2*, 1756−1764.
37. Matzapetakis, M., Farrer, B. T., Weng, T. C., Hemmingsen, L., Penner-Hahn, J. E., and Pecoraro, V. L. (2002) Comparison of the binding of cadmium(II), mercury(II), and arsenic(III) to the *de novo* designed peptides TRI L12C and TRI L16C, *J. Am. Chem. Soc. 124*, 8042−8054.
38. Claudio, E. S., Magyar, J. S., Godwin, H. A. (2003) *Prog. Inorg. Chem. 51*, 1−144.
39. Hemmingsen, L., Olsen, L., Antony, J., and Sauer, S. P. (2004) First principle calculations of ^{113}Cd chemical shifts for proteins and model systems, *J. Biol. Inorg. Chem. 9*, 591−599.
40. Bauer, R. J., S. J.; Schmidt-Nielsen. B. (1988) The angular overlap model applied to the calculation of nuclear quadrupole interactions. Derivation of partial nuclear quadrupole interaction parameters for biological relevant ligands in cadmium complexes. *Hyperfine Interact. 39*, 203−234.
41. Hemmingsen, L., Ryde, U., and Bauer, R. (1999) Nuclear quadrupole interactions in cadmium complexes: Semiempirical and *ab initio* calculations, *Z. Naturforsch., A: Phys. Sci. 54*, 422−430.
42. Anderson, A. C., O'Neil, R. H., DeLano, W. L., and Stroud, R. M. (1999) The structural mechanism for half-the-sites reactivity in an enzyme, thymidylate synthase, involves a relay of changes between subunits, *Biochemistry 38*, 13829−13836.
43. Biemann, H. P., and Koshland, D. E., Jr. (1994) Aspartate receptors of *Escherichia coli* and *Salmonella typhimurium* bind ligand with negative and half-of-the-sites cooperativity, *Biochemistry 33*, 629−634.
44. Kolodziej, A. F., Tan, T., and Koshland, D. E., Jr. (1996) Producing positive, negative, and no cooperativity by mutations at a single residue located at the subunit interface in the aspartate receptor of *Salmonella typhimurium*, *Biochemistry 35*, 14782−14792.
45. Helmann, J. D., Ballard, B. T., and Walsh, C. T. (1990) The MerR metalloregulatory protein binds mercuric ion as a tricoordinate, metal-bridged dimer, *Science 247*, 946−948.
46. Ansari, A. Z., Chael, M. L., and O'Halloran, T. V. (1992) Allosteric underwinding of DNA is a critical step in positive control of transcription by Hg-MerR, *Nature 355*, 87−88.
47. Sun, Y., Wong, M. D., and Rosen, B. P. (2002) Both metal binding sites in the homodimer are required for metalloregulation by the CadC repressor, *Mol. Microbiol. 44*, 1323−1329.
48. Apuy, J. L., Busenlehner, L. S., Russell, D. H., and Giedroc, D. P. (2004) Ratiometric pulsed alkylation mass spectrometry as a probe of thiolate reactivity in different metalloderivatives of *Staphylococcus aureus* pI258 CadC, *Biochemistry 43*, 3824−3834.
49. Beard, S. J., Hashim, R., Membrillo-Hernandez, J., Hughes, M. N., and Poole, R. K. (1997) Zinc(II) tolerance in *Escherichia coli* K-12: Evidence that the *zntA* gene (o732) encodes a cation transport ATPase, *Mol. Microbiol. 25*, 883−891.
50. Binet, M. R., and Poole, R. K. (2000) Cd^{II}, Pb^{II}, and Zn^{II} ions regulate expression of the metal-transporting P-type ATPase ZntA in *Escherichia coli*, *FEBS Lett. 473*, 67−70.
51. Brocklehurst, K. R., Hobman, J. L., Lawley, B., Blank, L., Marshall, S. J., Brown, N. L., and Morby, A. P. (1999) ZntR is a Zn^{II}-responsive MerR-like transcriptional regulator of *zntA* in *Escherichia coli*, *Mol. Microbiol. 31*, 893−902.
52. Yoon, K. P., Misra, T. K., and Silver, S. (1991) Regulation of the cadA cadmium resistance determinant of *Staphylococcus aureus* plasmid pI258, *J. Bacteriol. 173*, 7643−7649.
53. Coombs, J. M., and Barkay, T. (2004) Molecular evidence for the evolution of metal homeostasis genes by lateral gene transfer in bacteria from the deep terrestrial subsurface, *Appl. Environ. Microbiol. 70*, 1698−1707.

BI050094V